Geophysical Research Letters

RESEARCH LETTER
10.1029/2021GL097597

Key Points:

- High-speed auroral observations allow us to probe chorus wave properties in detail through the cyclotron resonance as flash aurora
- The temporal properties of flash aurora cannot be reproduced by the cyclotron resonance with an isolated lower-band chorus
- Auroral observations and computations suggest an isolated chorus element distributing up to the upper-band range in the source region

Supporting Information:

Supporting Information may be found in the online version of this article.

Correspondence to:

M. Ozaki,
ozaki@is.t.kanazawa-u.ac.jp

Citation:

Ozaki, M., Yagitani, S., Shiokawa, K., Tanaka, Y., Ogawa, Y., Hosokawa, K., et al. (2022). Slow contraction of flash aurora induced by an isolated chorus element ranging from lower-band to upper-band frequencies in the source region. *Geophysical Research Letters*, *49*, e2021GL097597. https://doi.org/10.1029/2021GL097597

Received 22 DEC 2021
Accepted 19 APR 2022

Slow Contraction of Flash Aurora Induced by an Isolated Chorus Element Ranging From Lower-Band to Upper-Band Frequencies in the Source Region

Mitsunori Ozaki[1], Satoshi Yagitani[1], Kazuo Shiokawa[2], Yoshimasa Tanaka[3,4,5], Yasunobu Ogawa[3,4,5], Keisuke Hosokawa[6], Yoshiya Kasahara[1], Yusuke Ebihara[7], Yoshizumi Miyoshi[2], Kousuke Imamura[1], Ryuho Kataoka[3,4], Shin-ichiro Oyama[2,3,8], Teppei Chida[1], and Akira Kadokura[3,4,5]

[1]Graduate School of Natural Science and Technology, Kanazawa University, Kanazawa, Japan, [2]Institute for Space-Earth Environmental Research, Nagoya University, Nagoya, Japan, [3]National Institute of Polar Research, Tachikawa, Japan, [4]Department of Polar Science, The Graduate University for Advanced Studies, SOKENDAI, Tachikawa, Japan, [5]Polar Environment Data Science Center, Joint Support-Center for Data Science Research, Research Organization of Information and Systems, Tachikawa, Japan, [6]The University of Electro-Communications, Chofu, Japan, [7]Research Institute for Sustainable Humanosphere, Kyoto University, Uji, Japan, [8]Space Physics and Astronomy Research Unit, University of Oulu, Oulu, Finland

Abstract Flash aurora driven by an isolated chorus element can be a useful ionospheric indicator for identifying the source wave properties via wave-particle interactions. Using ground observation and modeling approaches, here we report the temporal characteristics of flash aurora that depend on the chorus frequency width and the sweep rate. We found that the contraction time increases more than the expansion time in patchy auroral variations, due to the difference in the minimum electron energies resonated with the chorus wave packet away from the equatorial source to higher latitudes. Especially, the contraction time strongly depends on the higher-frequency chorus waves due to cyclotron resonance with lower-energy electrons. The model calculations support that the chorus element ranges from lower-band to upper-band frequencies with respect to half the gyrofrequency at the exact generation region. Our study provides the prompt (milliseconds) chorus-driven electron dynamics through the spatiotemporal characteristics of flash aurora in the ionosphere.

Plain Language Summary The wave frequency of a chorus wave, which is one of the electromagnetic wave emissions in magnetized plasmas, is an important parameter for characterizing energetic particles in the Earth's magnetosphere. Even though chorus waves are classified into two bands—lower- and upper-band frequencies separated at half the electron gyrofrequency—it is not well established that both lower- and upper-band chorus are essentially the same at the generation region. In this study, we investigate temporal characteristics of specific aurora caused by discrete chorus elements to identify the whole frequency band of chorus waves at the magnetospheric generation region. The aurora reflects the physical properties of the magnetospheric processes through the geomagnetic field lines from the generation region; thus, the aurora in the ionosphere becomes an ionospheric display on which the magnetospheric chorus waves are generated. Using auroral images along with model calculations, we find that the contraction time is longer than the expansion time as auroras vary their shape, depending on the frequency width of chorus wave packets. This study provides a new insight into the role of rapid (milliseconds) resonant interaction processes between discrete chorus elements and electrons over a wider energy range.

1. Introduction

Chorus waves, which are a kind of natural coherent emissions of plasma waves (W. Li et al., 2011; Omura, 2021; Santolík et al., 2003; Tsurutani & Smith, 1977), have attracted considerable attention due to their excellent acceleration of energetic electrons in the Earth's magnetosphere (Allison et al., 2021; Horne et al., 2005; Miyoshi et al., 2003; Omura et al., 2007; Summers et al., 2007; Thorne et al., 2013). A pure single chorus element can promptly accelerate seed electrons to energies of mega-electron-volts through wave-particle interactions (Foster et al., 2017). Additionally, an isolated chorus element can rapidly scatter energetic electrons over a very wide energy range in the magnetosphere into the loss cone, and then illuminate flash auroras in the ionosphere

(Ozaki et al., 2019). Chorus waves range in the frequency from 0.2 to 0.7f_{ce}, where f_{ce} is the equatorial electron gyrofrequency (Omura, 2021; Tsurutani & Smith, 1977). The frequency band is divided into two bands: lower-band (0.2–0.5f_{ce}) and upper-band (0.5–0.7f_{ce}) elements with respect to half the gyrofrequency (Gao et al., 2019; Tsurutani & Smith, 1974; Yagitani et al., 2014). Near the source region, observational studies frequently reported only the lower-band chorus (LBC) or both the lower-band chorus (LBC) and upper-band chorus (UBC) with a gap at half the gyrofrequency (Santolík et al., 2003), but some studies suggest that the lower-band chorus (LBC) and upper-band chorus (UBC) are continuously the same wave elements at an exact source region (Kurita et al., 2012; Omura et al., 2009). If an isolated chorus element ranging from lower-band to upper-band frequencies is generated at the equatorial source region, as suggested by a nonlinear wave growth theory (Omura et al., 2009), related temporal characteristics should be observed in the flash aurora that is driven by a pure single chorus wave packet. However, to date, there have been no auroral observations showing the temporal characteristics of flash aurora by existing an isolated chorus element ranging from lower-band to upper-band frequencies at the source; hence, the relationship between the chorus frequency range and aurora illumination by precipitating electrons is still poorly understood. One of the reasons is the requirement for a high temporal resolution in optical measurements due to the short duration (less than 1 s) of a typical discrete chorus element.

In this study, we overcome this difficulty using a recently developed electron multiplying charge coupled device (EMCCD) camera that enables continuous high-speed (100-Hz) observations. The high-speed auroral observations identify a preferential temporal property that patchy flash auroras show slower spatial contraction than expansion. Combining chorus-ray tracing in the magnetosphere and calculations of the auroral volume emission rate in the ionosphere, we show that the longer contraction time of flash aurora strongly suggests the results of cyclotron resonance of energetic electrons with a discrete chorus element distributing up to the upper-band range. Since the wave frequency is one of the essential parameters for determining the resonance energy of energetic electrons via wave-particle interactions (Kennel & Petschek, 1966), this study greatly contributes to the understanding of microphysics that underlie prompt particle acceleration and loss via chorus element wave-particle interactions.

2. Observations

2.1. Experimental Setup

Flash aurora has been classified into a kind of fast pulsating auroras because of chorus-driven electron precipitation (e.g., Nishimura et al., 2020; Oguti, 1978). Typical pulsating auroras show quasi-periodic luminous modulations related to a bundle of chorus elements (Kasahara et al., 2018; Miyoshi et al., 2010; Nishimura et al., 2020), but flash aurora shows a transient luminous response related to an isolated chorus element. The typical duration and patchy size of flash auroras are less than 1 s and less than 4,000 km^2, respectively (Ozaki et al., 2021). Kataoka et al. (2012) reported a rapid 54-Hz modulation in a standard periodic pulsating auroral event, but such rapid luminous modulations are different from the transient luminous emission of the isolated flash aurora. Our auroral observatory is placed in a favorable dark environment of the High-frequency Active Auroral Research Program (HAARP), Gakona, Alaska (62.41°N, 145.16°W), far from urban areas. We use a high-speed (100 Hz-sampling) EMCCD camera with a 665-nm long-pass glass filter, to monitor only the prompt (microsecond to nanosecond lifetimes) near-infrared emission lines of N2 (Hosokawa, Oyama, et al., 2020; Shiokawa et al., 2017). The temporal features of flash auroras were estimated using the level set method (C. Li et al., 2010; Osher & Sethian, 1988), which is a well-known image segmentation technique, especially for active contour models in medical imaging. The main advantages of the level set method are that it produces segmentation contours that are more robust, accurate, smooth, and closed than those produced by Otsu's method (Otsu, 1979). In this study, we analyzed 91 events of isolated flash aurora observed from 13:00 to 13:30 UT (02–03 MLT) on 30 March 2017. Electron precipitation events driven by chorus riser elements have been reported in this period (Hosokawa, Miyoshi, et al., 2020; Ozaki et al., 2018), so we quantitatively evaluated the temporal characteristics of flash auroras related to chorus riser elements.

2.2. Observation Results

Figures 1a and 1b show the time-sequential images and auroral size, respectively, of a typical patchy flash aurora with the projection at an altitude of 110 km (see Text S1 in Supporting Information S1). The typical flash aurora

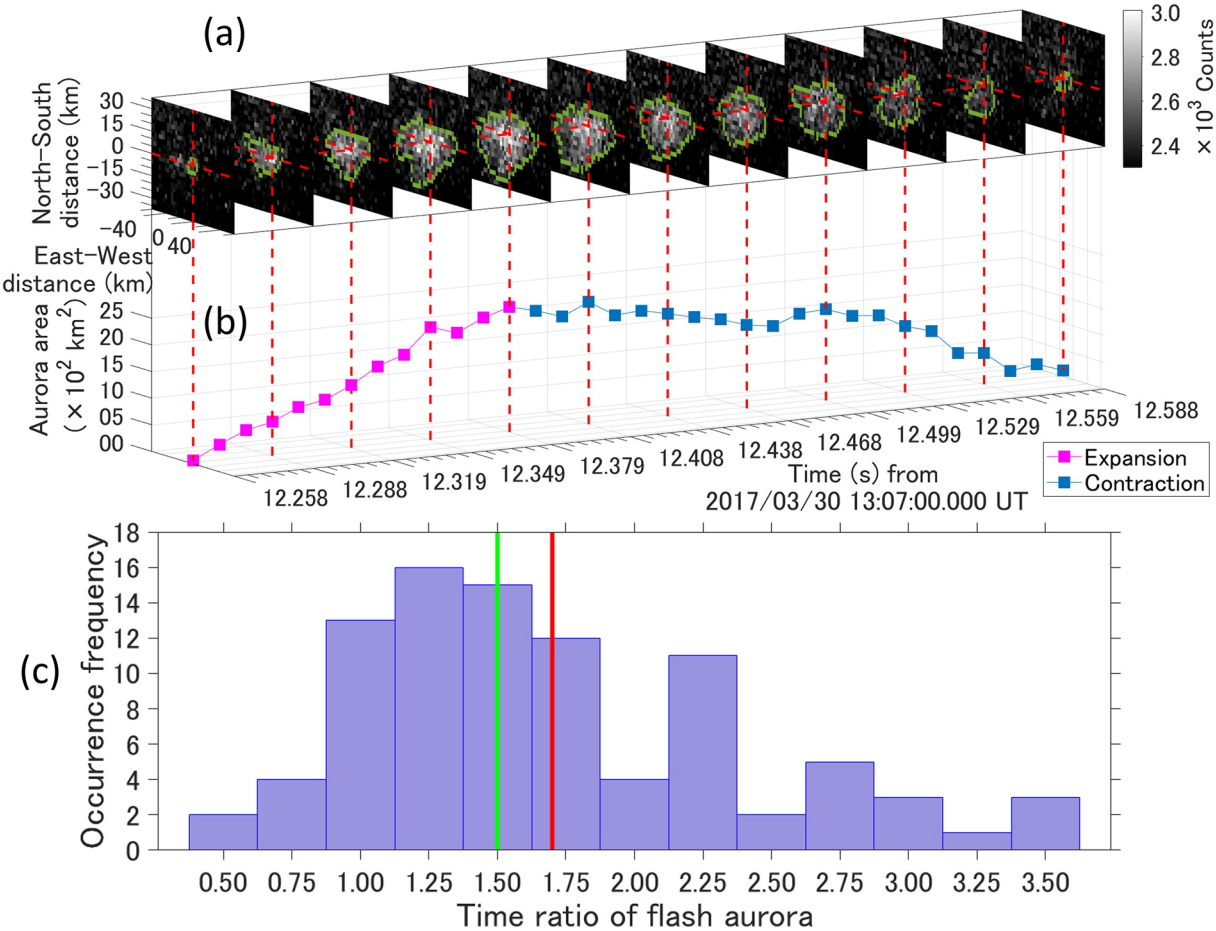

Figure 1. (a) Time-sequential images and (b) spatial size variations of a typical flash aurora in the ionosphere. Green closed paths in each image indicate the outline of a flash aurora. (c) Histogram of the time ratio of morphological contraction to expansion of flash auroras. Green and red bars indicate the median and average values, respectively.

shows morphological expansion and contraction variations. The spatial evolutions provide temporal characteristics of expansion (initial emission to auroral emission at the maximum patchy size) and contraction (auroral emission at the maximum patchy size to final emission). We should use a time ratio of spatial contraction to expansion in each auroral event to mitigate the effects that different events occur at different locations in the field of view. The time ratio of spatial contraction to expansion of flash auroras is plotted in Figure 1c. Seventy-two of the 91 flash auroras show a longer contraction time. That is, the contraction time is significantly longer than the expansion (in which temporal ratio >1). The average and median of the time ratio are 1.7 and 1.5, respectively. In these events, the maximum (minimum) expansion and contraction times are 0.45 (0.06) s and 0.65 (0.05) s, respectively. A 665-nm long-pass glass filter was used in the optical observations, so the observations can reflect the temporal characteristics of an isolated chorus element in the magnetosphere through the prompt auroral emissions at the N2 first positive bands in the ionosphere.

If the flash aurora results from resonant scattering of electrons with individual chorus elements, there will be some dominant physical processes or parameters that determine the preferential longer contraction time. If the electron density is assumed to be constant along the field line in a narrow range of cyclotron resonance, the minimum resonance energy is characterized by the highest frequency of whistler-mode chorus waves (Kennel & Petschek, 1966) at the equator. The observed temporal property of the longer contraction can reflect the frequency band of chorus elements at the source region in the equatorial magnetosphere.

3. Numerical Analysis

3.1. Analytical Model

We simply consider parallel wave propagation and the travel of energetic particles along a geomagnetic field line based on the model by Miyoshi et al. (2010) to cause the flash aurora. Let us assume that the energetic electrons having a parallel velocity $v_p(f, s)$ resonate with chorus waves, and a parallel group velocity of chorus waves is expressed as $v_g(f)$ in a simple case of a constant electron density along the geomagnetic field line, where f is the chorus wave frequency and s is the distance along the geomagnetic field line. The maximum spatial extent of flash aurora is determined by the resonance location at the highest latitude point s_1 with the highest chorus frequency f_{ch} because of spreading chorus rays. The expansion time T_e of flash aurora can be written as

$$T_e = \int_{s_1}^{s_{iono}} \frac{\mathrm{d}s}{v_p(f_{ch}, s_1)} - \int_{s_{eq}}^{s_{iono}} \frac{\mathrm{d}s}{v_p(f_{cl}, s_{eq})} + \frac{f_w}{\frac{\mathrm{d}f}{\mathrm{d}t}} + \int_{s_{eq}}^{s_1} \frac{\mathrm{d}s}{v_g(f_{ch})}, \tag{1}$$

where s_{iono} and s_{eq} are a location in the ionosphere and an equatorial location (source), respectively, and f_{cl}, $f_w = f_{ch} - f_{cl}$, and $\mathrm{d}f/\mathrm{d}t$ are the lowest wave frequency, the bandwidth, and the frequency sweep rate of a chorus element, respectively. The first term is the traveling time of the minimum energy electrons at s_1, which can characterize the maximum size of a patchy flash aurora by spreading chorus rays. The second term is the traveling time of the highest energy electrons at the source, which can contribute to the initial auroral emission. The time duration of the chorus riser element in the third term and the wave propagation time in the fourth term should be considered. While the expansion time is not simply related to the chorus sweep rate, the effects of the sweep rate and the highest-frequency chorus are potentially included. Next, the contraction time T_c of flash aurora is written as

$$T_c = \int_{s_{eq}}^{s_{iono}} \frac{\mathrm{d}s}{v_p(f_{ch}, s_{eq})} - \int_{s_1}^{s_{iono}} \frac{\mathrm{d}s}{v_p(f_{ch}, s_1)} - \int_{s_{eq}}^{s_1} \frac{\mathrm{d}s}{v_g(f_{ch})}, \tag{2}$$

$$\approx \int_{s_{eq}}^{s_{iono}} \frac{\mathrm{d}s}{v_p(f_{ch}, s_{eq})} - \int_{s_1}^{s_{iono}} \frac{\mathrm{d}s}{v_p(f_{ch}, s_1)}. \tag{3}$$

The propagation time of the chorus wave packet from the equator to a higher latitude (location s_1) in term 3 in Equation 2 is the smallest term because $\int_{s_{eq}}^{s_1} \mathrm{d}s$ (~3,000 km in $L = 5.5$ to 6) is a much smaller distance than $\int_{s_{eq}}^{s_{iono}} \mathrm{d}s$ (~50,000 km in $L = 5.5$ to 6). The first term in Equation 2 is the traveling time of the minimum energy electrons at the equator, which can characterize the final contraction size of a patchy flash aurora. The contraction time is not related to the chorus sweep rate, but it should be determined by the highest-frequency chorus. Thus, taking a higher sweep rate and a higher wave frequency becomes a better condition for satisfying the observed condition $T_e < T_c$, from Equations 1 and 3.

3.2. Numerical Model

To assess whether the temporal characteristics of flash aurora reflect the chorus wave properties, we used a model calculation that included the effects of nonducted wave propagation in detail. The model calculation is the same as Ozaki et al. (2021). The electron density (see Figure S1 in Supporting Information S1), geomagnetic field line, and energetic electron flux are used from the GCPM 2.2 (Gallagher et al., 2000), Tsyganenko 2002 (Tsyganenko, 2002), and AE9 (Ginet et al., 2013) models applied for the observation time, respectively. Static snapshots of chorus source size (transverse to the background field line) have been reported in various (tens- to hundreds-kilometers) scales by multiple satellite observations of discrete chorus elements (e.g., Agapitov et al., 2017; Santolík & Gurnett, 2003; Shen et al., 2019). The chorus source size can have a spatial evolution as represented by the spatial development of flash aurora. A point source is assumed to be a chorus source model, because the final flash aurora shows a spatially confined region (see the final frame in Figure 1a). The final contraction scale can be characterized by the minimum resonance energy at the equator because of the slowest traveling time to the ionosphere. The steady and small amplitude whistler mode waves may distribute in a wide spatial range in the magnetosphere, but they are not chorus waves through a nonlinear wave growth gaining a

sufficiently large amplitude. We therefore assume that the transverse size of the chorus wave-particle interaction region can be localized, because the final contraction spot of flash aurora is clearly brighter than the background level. On the other hand, a possibility of a time varying source size at the equator is the future work. The column emission rate (CER) of 670.5 nm in the N2 first positive band is calculated using a two-stream approximation model by Ono (1993) for the energetic electrons satisfying the first cyclotron resonance with the chorus rays (Bortnik et al., 2006b). Our model does not include the effects of pitch angle changes and precipitating flux values related to chorus wave intensities (Ni et al., 2016) to simplify the calculation with limited computing resources. These effects are important for estimating the auroral luminosity, but are not essential for estimating the temporal characteristics of auroral emissions under the assumption that an isolated chorus element shows a sufficiently large amplitude in the whole frequency band. In addition, our model calculation does not include the effects of nonlinear damping in the frequency range from half the gyrofrequency at the equator (exact generation region) to half the local gyrofrequency at higher latitudes associated with the wave propagation (Yagitani et al., 2014). Because the latitudinal range of cyclotron resonance is less than several degrees and the maximum frequency ($0.7f_{ce}$) of upper-band chorus (UBC) is larger than half the local gyrofrequency along the field line, our model calculation is considered to be appropriate for estimation of temporal characteristics of auroral emissions scattered by the modeled chorus rays.

3.3. Computation Results

Numerous chorus rays are launched toward the Southern Hemisphere with an initial wave normal angle (WNA) width of 10°, a frequency sweep rate of 20 kHz/s, and resonance latitudes up to 5° from the magnetic equator at $L = 5.78$ as shown in Figure 2a. Other parameters are listed in Table S1 in Supporting Information S1. In the case of LBC ($0.2–0.5f_{ce}$) injection, the temporal evolutions of the calculated CER, the precipitating electron energy, and the resonated chorus frequency are plotted in three panels of Figure 2b. The injection of both LBC and UBC ($0.2–0.7f_{ce}$) are plotted in the same format in three panels of Figure 2c. The UBC can more easily propagate to lower L-shells than the LBC in the nonducted mode (see Movie S1), so the horizontal spatial development of the CER is smaller for the LBC. The difference in propagation characteristics between LBC and UBC is consistent with the results of previous ray tracing studies (e.g., Bortnik et al., 2006a; Yamaguchi et al., 2013). The maximum development toward the north-south direction in Figure 2b is 0.27 times smaller in comparison with Figure 2c (north-south and east-west ranges are different in both figures). An asymmetric CER evolution in the north-south direction is emphasized by the UBC propagation toward lower L-shells, but the northward CER evolution is not sufficiently controlled by both LBC and UBC propagation in comparison with Figure 1a. Although the northward (higher latitude) development of the observed flash aurora is a minor variation in comparison with the southward (lower latitude) development, the northward development will be refined using a more precise source model instead of a point source in future work. In the auroral expansion phase, the precipitating electron energy and chorus frequency become gradually lower and higher, respectively, as the analytical model by expression (1). This temporal energy variation can be interpreted as an energy dispersion in agreement with the energy spectra of pulsating aurora (Miyoshi et al., 2010, 2015). In the auroral contraction phase, the resonance energy and chorus frequency remain almost constant to be the lowest energy and the highest chorus frequency, respectively. Thus, our computations support the idea that the temporal characteristics in the contraction phase depend on the difference in the traveling time of energetic electrons caused by cyclotron resonance from the source to higher latitudes with the highest-frequency chorus, as the analytical model in the approximate expression (3).

Figure 3 shows the temporal characteristics of the CER as a function of the maximum chorus frequency with different chorus sweep rates. Because the distribution of chorus sweep rates is from several to a few tens of kilohertz per second at $L = 4.5$ to 5.5 (subauroral latitudes) in satellite observations (Macúšová et al., 2010; Titova et al., 2003), we assumed three cases of sweep rates (5, 10, and 20 kHz/s). Other calculation parameters are the same as those listed in Table S1 in Supporting Information S1. In all cases, our computations show that a discrete chorus element distributing up to the upper-band range is required to reconstruct the observed longer contraction with a time ratio >1. The time ratio takes a larger value when the chorus sweep rate increases. This can be explained by the expansion time decrease becoming lower when the sweep rate is higher in Equation 1. The time ratio in Figure 3 is smaller than the averaged observation value of 1.7, but the time ratio is also controlled by initial WNAs and resonance latitudes as shown in Figure 4.

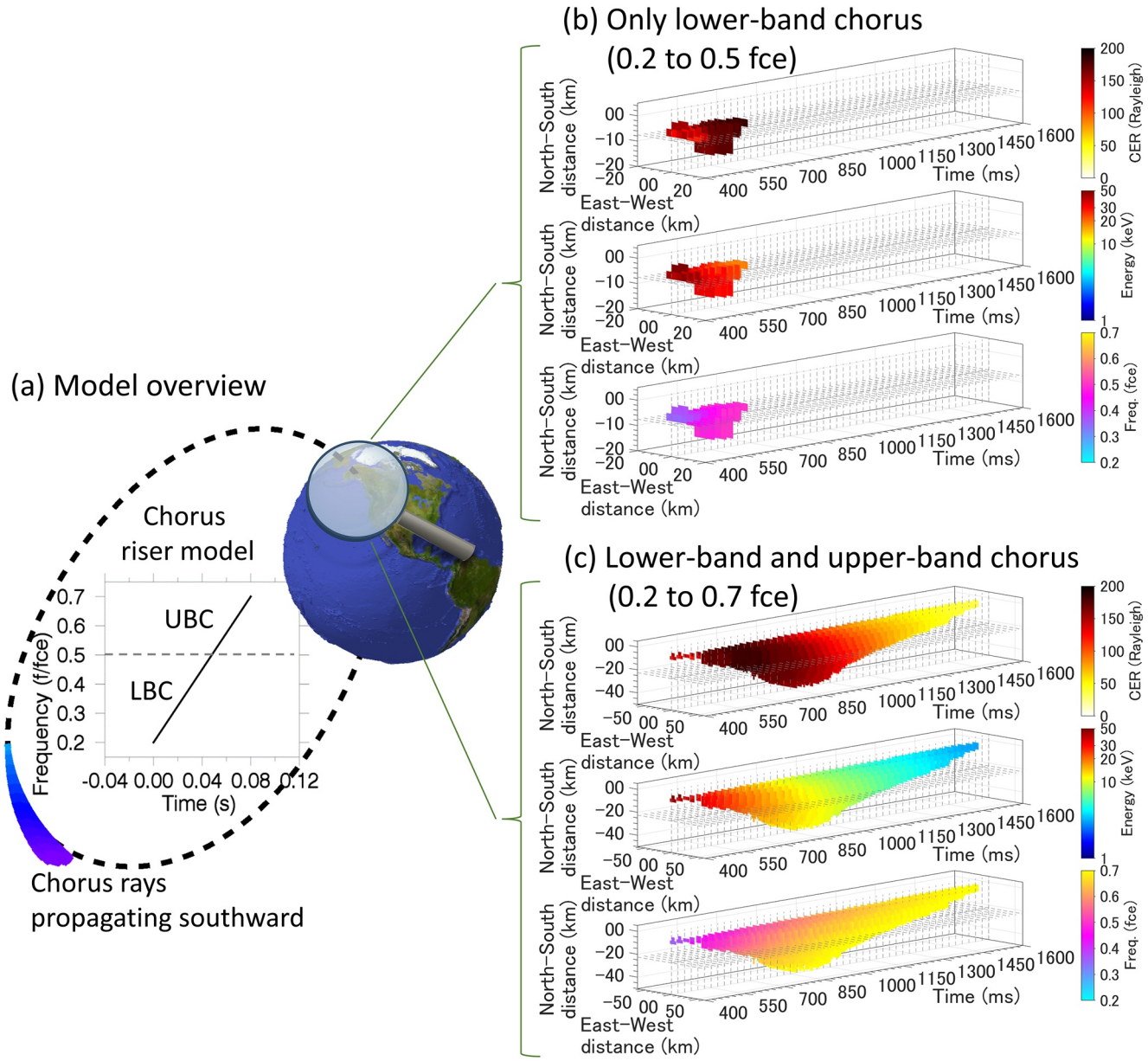

Figure 2. (a) Model overview, and (b and c) spatiotemporal evolutions (every 25 ms) of calculated flash auroras in the ionosphere for cases of the lower-band chorus (LBC) only and both the LBC and upper-band chorus, respectively. A time value of zero means the chorus injection time. Spatial evolutions of chorus rays and column emission rate as virtual flash aurora are seen in Movie S1, S2, and S3.

Finally, the maximum spatial size (top panels in Figures 4a and 4b) and the temporal characteristics (bottom panels in Figures 4a and 4b) of the CER as functions of the initial WNA width and resonance latitudes were evaluated. The maximum spatial size of the CER increases with increasing initial WNA and resonance latitudes independent of the chorus sweep rate because the spatial size can be constrained by chorus rays spreading away from the source region to higher latitudes. Chorus rays injected from the equatorial source spread more when the initial WNA was wider and resonance latitudes were wider along the field lines. The effects of spreading chorus rays contribute to the larger spatial extent of the wave-particle interaction region at higher L-shells deduced from chorus-driven pulsating auroras at high (~8) L shells (Nishimura et al., 2011) and at a low (~5) L shell in auroral latitudes (Ozaki et al., 2018) because chorus rays will have larger extent during their injection at higher L-shells playing a key propagation effect. In each chorus sweep rate, the time ratio displays a remarkable increase with increasing resonance latitudes for a constant initial WNA. If the chorus propagation is a major factor with

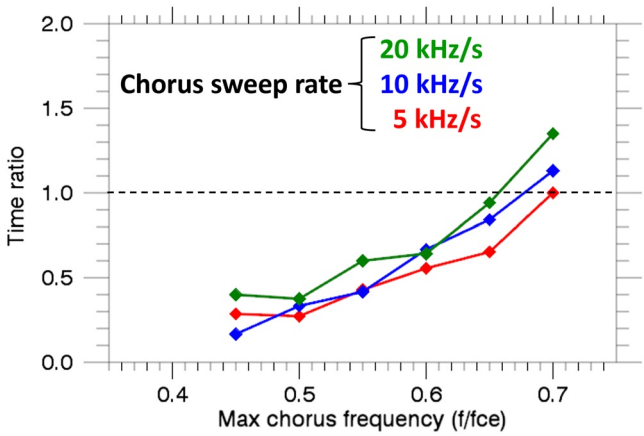

Figure 3. Time ratio of spatial contraction to expansion of the calculated column emission rate as a function of the maximum chorus frequency. The lowest chorus frequency is $0.2f_{ce}$ in each calculation.

increasing resonance latitudes, the time ratio cannot increase with increasing chorus propagation time in the fourth term of Equation 1. The increase of the time ratio with increasing resonance latitudes is caused by the smaller energy difference between the first and second terms in Equation 1.

We focus on the temporal characteristics at spatial sizes smaller than 4,000 km^2 based on a statistical study of flash auroral size by Ozaki et al. (2021). Figure 4a summarizes the maximum spatial size of the CER and the time ratio in case for the LBC injection. The area is less than 4,000 km^2, but the time ratio is less than 1.7. This means that we hardly explain the time ratio being greater than 1.7 for the parameters that we surveyed. Figure 4b is the same as Figure 4a except for the case that the LBC and UBC are injected. In comparison with Figure 4a, the area and the time ratio are larger, but the area under conditions of large WNAs and wide resonance latitudes are inconsistent with the observed auroral sizes. This difference in the spatial size between the calculated CER and the observations could come from the difference in the LBC and UBC propagation characteristics. UBC in the inner magnetosphere is largely confined to within ~6° as distinct from LBC in the global chorus morphology (Meredith et al., 2012), and UBC is strongly attenuated by Landau damping with the oblique propagation (Bortnik & Thorne, 2007). Calculations in the LBC and UBC with the WNAs from 5 to 8° and the resonance latitude of 6° for the sweep rates of 10 and 20 kHz/s and with the WNAs from 5 to 6° and the resonance latitude of 7° for the sweep rate of 5 kHz/s correctly satisfied both conditions of the spatial size <4,000 km^2 and the time ratio between 1.5 and 1.7. These calculations suggest that an isolated chorus element ranging from lower-band to upper-band frequencies with quasi-parallel propagation at the source region gives a reasonable cause for forming the observed slow contraction of flash aurora. We used a point wave source, but the multiple satellite observations have reported larger chorus sources over hundreds-km transverse scales (Agapitov et al., 2017; Shen et al., 2019). Chorus rays emitted by such a larger source give more spreading rays than those from a point source. Chorus waves from a larger source also suggest more parallel propagation with smaller WNAs to confine the spatial scale of flash aurora <4,000 km^2.

4. Summary and Discussion

Our high-speed auroral observations and computations highlight the generation of discrete chorus elements distributed up to the upper-band frequency in the exact source region. Hosokawa, Miyoshi, et al. (2020) and Ozaki et al. (2018, 2019) showed that each LBC wave packet creates each patchy auroral emission from the conjugate Arase and ground observations, but the LBCs without UBCs were observed at the magnetic latitude of ~20° in their studies. The high-speed auroral imaging observations shed light upon the equatorial chorus wave properties, which are not expected from their conjugate observations. The effects of UBC on the auroral emissions will be demonstrated by conjugate observations of equatorial chorus waves and auroral emissions in the future. Since an isolated chorus element ranging from lower-band to upper-band frequencies is required at the magnetic equator in this study, the evolution of the wave gap at $0.5f_{ce}$ and a disappearance of UBC at a satellite location far from the equator could be caused by the chorus wave propagation away from the source to higher latitudes. This situation agrees with the nonlinear damping in the frequency range from half the gyrofrequency at the equator to half the local gyrofrequency at higher latitudes associated with the wave propagation (Yagitani et al., 2014). Consideration of the effects of the nonlinear wave damping using a realistic wave amplitude is a subject for future study. However, our conclusion that a discrete chorus element distributing up to the upper-band range at the equator is required for reconstructing the time ratio (larger than 1) of flash aurora remains the same, since the auroral shrinking variation is strongly characterized by the cyclotron resonance with UBC as shown in Figure 2, regardless of the effects of nonlinear damping. Our conclusion is based on the model calculation using a point source from the final contraction spot of flash aurora. Our study supports the observations of a small transverse spatial (tens up to 100 km) scale of an isolated chorus source size by, for example, Santolík and Gurnett (2003), among a variety of spatial scales.

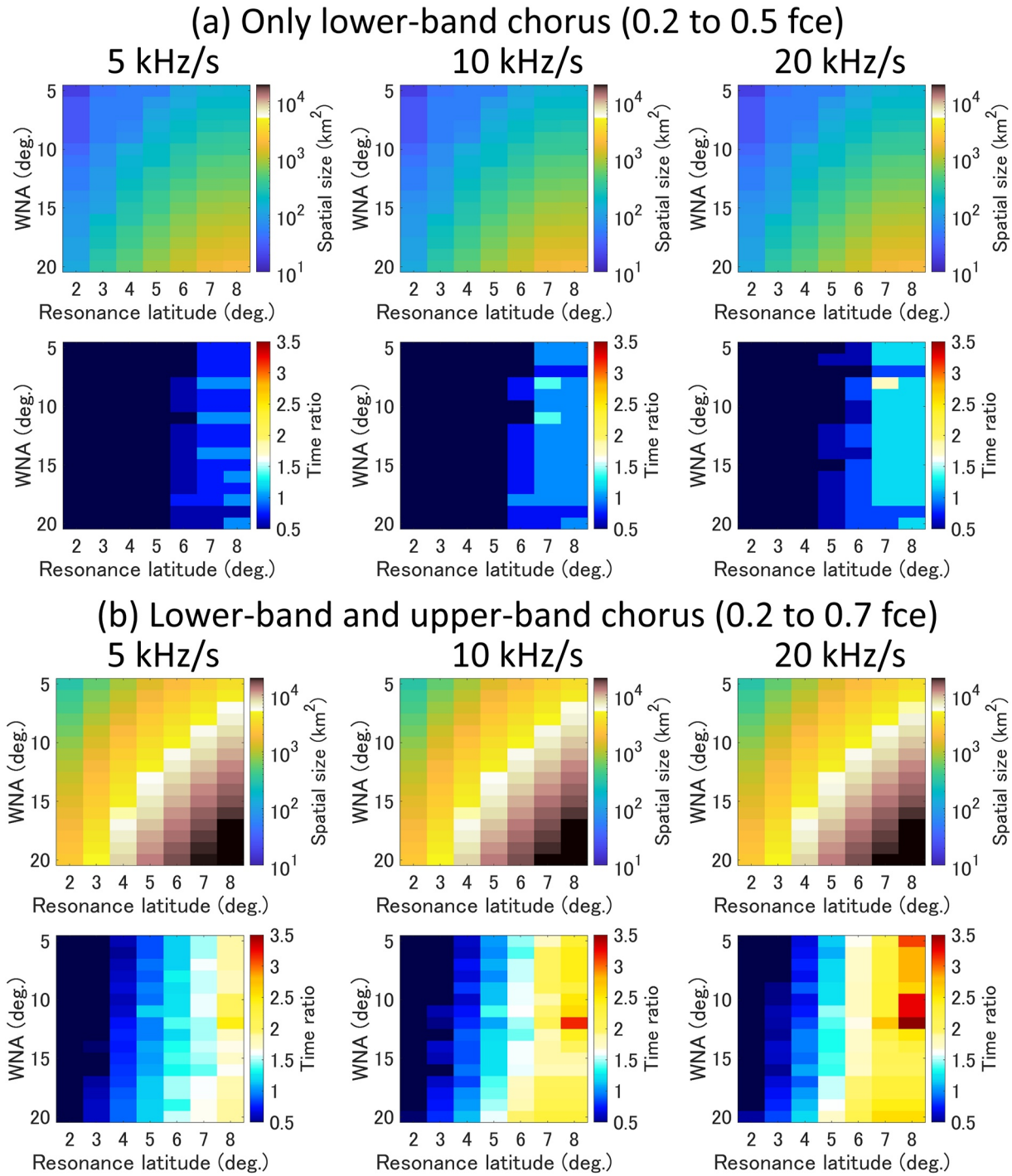

Figure 4. Evaluation of the maximum spatial size and the temporal characteristics (time ratio of spatial contraction to expansion) of the column emission rate as functions of the initial wave normal angle and resonance latitudes for the different chorus sweep rates.

Most satellite observations show dual-band chorus (DBC) waves with a gap at $0.5f_{ce}$ (Gao et al., 2019), and many mechanisms for generating the dual-band chorus (DBC) have been suggested, including Landau damping (Bortnik et al., 2006b; Tsurutani & Smith, 1974), nonlinear damping (Omura et al., 2009; Yagitani et al., 2014), different resonances (J. Li et al., 2019), and different sources (Bell et al., 2009) and so on. If a dual-band chorus (DBC) with a gap (width of $0.07f_{ce}$, as suggested by Gao et al., 2019) at half the gyrofrequency is injected at the generation region, the auroral CER caused by the DBC would show unnatural quenching in the spatial expansion (see

Figure S2 in Supporting Information S1) of virtual flash aurora due to nonresonance at the frequency gap. We can identify such a DBC at the source from the flash aurora in the spatial expansion, but as shown in Figures 1a and 1b, flash auroras usually show continuous spatial expansion without quenching.

In summary, this study supports that chorus elements at the exact source regions range from lower- to upper-band frequencies without a gap (Kurita et al., 2012) or with a quite narrower gap in comparison with $0.07f_{ce}$-width modeled by Gao et al. (2019) around half the gyrofrequency. After the wave excitation at the source, the DBC can be caused by wave damping (Omura et al., 2009; Tsurutani & Smith, 1974) and/or differential wave growth (J. Li et al., 2019; Ratcliffe & Watt, 2017) away from the source to higher latitudes. This should motivate future studies on the global energy dissipation of energetic electrons via the prompt responses of LBC and UBC wave-particle interactions.

Data Availability Statement

The EMCCD data (https://doi.org/10.34515/DATA.GND-0013-0006-0207_v01) we used to support the findings of this study were obtained from a link "100 Hz All-Sky imager data" in the ERG Science Center operated by ISAS/JAXA and ISEE/Nagoya University (http://ergsc.isee.nagoya-u.ac.jp/data_info/ground.shtml.en). The EMCCD data release is partly supported by the IUGONET (Inter-university Upper atmosphere Global Observation NETwork) project (http://www.iugonet.org/). The ray tracing model and the CER calculation are presented by Ozaki et al. (2021).

Acknowledgments
This study was supported by JSPS KAKENHI grants JP15H05747, JP16H06286, and JP20H02162. The authors would like to thank Dr. Yoshitaka Goto and Tomohiro Inoue for their helpful discussions on chorus-ray tracing and Toki Genda and Shion Hashimoto for their support on auroral image analysis. We appreciate Yuka Yamamoto and Takumi Adachi of Nagoya University for their skillful technical support for continuous operation of the all-sky camera at Gakona.

References

Agapitov, O., Blum, L. W., Mozer, F. S., Bonnell, J. W., & Wygant, J. (2017). Chorus whistler wave source scales as determined from multipoint Van Allen Probe measurements. *Geophysical Research Letters*, *44*(6), 2634–2642. https://doi.org/10.1002/2017GL072701

Allison, H. J., Shprits, Y. Y., Zhelavskaya, I. S., Wang, D., & Smirnov, A. G. (2021). Gyroresonant wave-particle interactions with chorus waves during extreme depletions of plasma density in the Van Allen radiation belts. *Science Advances*, *7*, 5. https://doi.org/10.1126/sciadv.abc0380

Bell, T. F., Inan, U. S., Haque, N., & Pickett, J. S. (2009). Source regions of banded chorus. *Geophysical Research Letters*, *36*(11), L11101. https://doi.org/10.1029/2009GL037629

Bortnik, J., Inan, U. S., & Bell, T. F. (2006a). Landau damping and resultant unidirectional propagation of chorus waves. *Geophysical Research Letters*, *33*(3), L03102. https://doi.org/10.1029/2005GL024553

Bortnik, J., Inan, U. S., & Bell, T. F. (2006b). Temporal signatures of radiation belt electron precipitation induced by lightning-generated MR whistler waves: 1. Methodology. *Journal of Geophysical Research*, *111*(A2), A02204. https://doi.org/10.1029/2005JA011182

Bortnik, J., & Thorne, R. M. (2007). The dual role of ELF/VLF chorus waves in the acceleration and precipitation of radiation belt electrons. *Journal of Atmospheric and Solar-Terrestrial Physics*, *69*, 3–386. https://doi.org/10.1016/j.jastp.2006.05.030

Foster, J. C., Erickson, P. J., Omura, Y., Baker, D. N., Kletzing, C. A., & Claudepierre, S. G. (2017). Van Allen Probes observations of prompt MeV radiation belt electron acceleration in nonlinear interactions with VLF chorus. *Journal of Geophysical Research: Space Physics*, *122*(1), 324–339. https://doi.org/10.1002/2016JA023429

Gallagher, D. L., Craven, P. D., & Comfort, R. H. (2000). Global core plasma model. *Journal of Geophysical Research*, *105*(A8), 18819–18833. https://doi.org/10.1029/1999JA000241

Gao, X., Chen, L., Li, W., Lu, Q., & Wang, S. (2019). Statistical results of the power gap between lower-band and upper-band chorus waves. *Geophysical Research Letters*, *46*(8), 4098–4105. https://doi.org/10.1029/2019GL082140

Ginet, G. P., O'Brien, T. P., Huston, S. L., Johnston, W. R., Guild, T. B., Friedel, R., et al. (2013). AE9, AP9 and SPM: New models for specifying the trapped energetic particle and space plasma environment. *Space Science Reviews*, *179*(1–4), 579–615. https://doi.org/10.1007/978-1-4899-7433-4_18

Horne, R. B., Thorne, R. M., Glauert, S. A., Albert, J. M., Meredith, N. P., & Anderson, R. R. (2005). Timescale for radiation belt electron acceleration by whistler mode chorus waves. *Journal of Geophysical Research*, *110*(A3), A03225. https://doi.org/10.1029/2004JA010811

Hosokawa, K., Miyoshi, Y., Ozaki, M., Oyama, S. I., Ogawa, Y., Kurita, S., et al. (2020). Multiple time-scale beats in aurora: Precise orchestration via magnetospheric chorus waves. *Scientific Reports*, *10*(1), 3380. https://doi.org/10.1038/s41598-020-59642-8

Hosokawa, K., Oyama, S., Ogawa, Y., Miyoshi, Y., Kurita, S., Teramoto, M., et al. (2020). A ground-based instrument suite for integrated high-time resolution measurements of pulsating aurora with Arase. *Earth and Space Science Open Archive*. https://doi.org/10.1002/essoar.10504721.1

Kasahara, S., Miyoshi, Y., Yokota, S., Mitani, T., Kasahara, Y., Matsuda, S., et al. (2018). Pulsating aurora from electron scattering by chorus waves. *Nature*, *554*(7692), 337–340. https://doi.org/10.1038/nature25505

Kataoka, R., Miyoshi, Y., Hampton, D., Ishii, T., & Kozako, H. (2012). Pulsating aurora beyond the ultra-low-frequency range. *Journal of Geophysical Research*, *117*(A8), A08336. https://doi.org/10.1029/2012JA017987

Kennel, C. F., & Petschek, H. E. (1966). Limit on stably trapped particle fluxes. *Journal of Geophysical Research*, *71*(1), 1–28. https://doi.org/10.1029/JZ071i001p00001

Kurita, S., Katoh, Y., Omura, Y., Angelopoulos, V., Cully, C. M., Le Contel, O., & Misawa, H. (2012). THEMIS observation of chorus elements without a gap at half the gyrofrequency. *Journal of Geophysical Research*, *117*(A11), A11223. https://doi.org/10.1029/2012JA018076

Li, C., Xu, C., Gui, C., & Fox, M. D. (2010). Distance regularized level set evolution and its application to image segmentation. *IEEE Transactions on Image Processing*, *19*(12), 3243–3254. https://doi.org/10.1109/tip.2010.2069690

Li, J., Bortnik, J., An, X., Li, W., Angelopoulos, V., Thorne, R. M., et al. (2019). Origin of two-band chorus in the radiation belt of Earth. *Nature Communications*, *10*(1), 4672. https://doi.org/10.1038/s41467-019-12561-3

Li, W., Bortnik, J., Thorne, R. M., & Angelopoulos, V. (2011). Global distribution of wave amplitudes and wave normal angles of chorus waves using THEMIS wave observations. *Journal of Geophysical Research*, *116*(A12), A12205. https://doi.org/10.1029/2011JA017035

Macúšová, E., Santolik, O., Decreau, P., Demekhov, A. G., Nunn, D., Gurnett, D. A., et al. (2010). Observations of the relationship between frequency sweep rates of chorus wave packets and plasma density. *Journal of Geophysical Research*, *115*(A12), A12257. https://doi.org/10.1029/2010JA015468

Meredith, N. P., Horne, R. B., Sicard-Piet, A., Boscher, D., Yearby, K. H., Li, W., & Thorne, R. M. (2012). Global model of lower band and upper band chorus from multiple satellite observations. *Journal of Geophysical Research*, *117*(A10), A10225. https://doi.org/10.1029/2012JA017978

Miyoshi, Y., Katoh, Y., Nishiyama, T., Sakanoi, T., Asamura, K., & Hirahara, M. (2010). Time of flight analysis of pulsating aurora electrons, considering wave-particle interactions with propagating whistler mode waves. *Journal of Geophysical Research*, *115*(A10), A10312. https://doi.org/10.1029/2009JA015127

Miyoshi, Y., Morioka, A., Obara, T., Misawa, H., Nagai, T., & Kasahara, Y. (2003). Rebuilding process of the outer radiation belt during the 3 November 1993 magnetic storm: NOAA and Exos-D observations. *Journal of Geophysical Research*, *108*(A1), 1004. https://doi.org/10.1029/2001JA007542

Miyoshi, Y., Saito, S., Seki, K., Nishiyama, T., Kataoka, R., Asamura, K., et al. (2015). Relation between fine structure of energy spectra for pulsating aurora electrons and frequency spectra of whistler mode chorus waves. *Journal of Geophysical Research: Space Physics*, *120*(9), 7728–7736. https://doi.org/10.1002/2015JA021562

Ni, B., Thorne, R. M., Zhang, X., Bortnik, J., Pu, Z., Xie, L., et al. (2016). Origins of the Earth's diffuse auroral precipitation. *Space Science Reviews*, *200*(1–4), 205–259. https://doi.org/10.1007/s11214-016-0234-7

Nishimura, Y., Bortnik, J., Li, W., Thorne, R. M., Chen, L., Lyons, L. R., et al. (2011). Multievent study of the correlation between pulsating aurora and whistler mode chorus emissions. *Journal of Geophysical Research*, *116*(A11), A11221. https://doi.org/10.1029/2011JA016876

Nishimura, Y., Lessard, M. R., Katoh, Y., Miyoshi, Y., Grono, E., Partamies, N., et al. (2020). Diffuse and pulsating aurora. *Space Science Reviews*, *216*, 1. https://doi.org/10.1007/s11214-019-0629-3

Oguti, T. (1978). Observations of rapid auroral fluctuations. *Journal of Geomagnetism and Geoelectricity*, *30*(4), 299–314. https://doi.org/10.5636/jgg.30.299

Omura, Y. (2021). Nonlinear wave growth theory of whistler-mode chorus and hiss emissions in the magnetosphere. *Earth Planets and Space*, *73*(1), 95. https://doi.org/10.1186/s40623-021-01380-w

Omura, Y., Furuya, N., & Summers, D. (2007). Relativistic turning acceleration of resonant electrons by coherent whistler mode waves in a dipole magnetic field. *Journal of Geophysical Research*, *112*(A6), A06236. https://doi.org/10.1029/2006JA012243

Omura, Y., Hikishima, M., Katoh, Y., Summers, D., & Yagitani, S. (2009). Nonlinear mechanisms of lower-band and upper-band VLF chorus emissions in the magnetosphere. *Journal of Geophysical Research*, *114*(A7), A07217. https://doi.org/10.1029/2009JA014206

Ono, T. (1993). Derivation of energy parameters of precipitating auroral electrons by using the intensity ratios of auroral emissions. *Journal of Geomagnetism and Geoelectricity*, *45*(6), 455–472. https://doi.org/10.5636/jgg.45.455

Osher, S., & Sethian, J. A. (1988). Fronts propagating with curvature-dependent speed: Algorithms based on Hamilton-Jacobi formulations. *Journal of Computational Physics*, *79*(1), 12–49. https://doi.org/10.1016/0021-9991(88)90002-2

Otsu, N. (1979). A threshold selection method from gray-level histograms. *IEEE Transactions on Systems, Man, and Cybernetics*, *9*(1), 62–66. https://doi.org/10.1109/TSMC.1979.4310076

Ozaki, M., Inoue, T., Tanaka, Y., Yagitani, S., Kasahara, Y., Shiokawa, K., et al. (2021). Spatial evolution of wave-particle interaction region deduced from flash-type auroras and chorus-ray tracing. *Journal of Geophysical Research: Space Physics*, *126*(7), e2021JA029254. https://doi.org/10.1029/2021JA029254

Ozaki, M., Miyoshi, Y., Shiokawa, K., Hosokawa, K., Oyama, S. i., Kataoka, R., et al. (2019). Visualization of rapid electron precipitation via chorus element wave–particle interactions. *Nature Communications*, *10*(1), 257. https://doi.org/10.1038/s41467-018-07996-z

Ozaki, M., Shiokawa, K., Miyoshi, Y., Hosokawa, K., Oyama, S., Yagitani, S., et al. (2018). Microscopic observations of pulsating aurora associated with chorus element structures: Coordinated Arase satellite-PWING observations. *Geophysical Research Letters*, *45*(22), 12125–12134. https://doi.org/10.1029/2018GL079812

Ratcliffe, H., & Watt, C. E. J. (2017). Self-consistent formation of a 0.5 cyclotron frequency gap in magnetospheric whistler mode waves. *Journal of Geophysical Research: Space Physics*, *122*(8), 8166–8180. https://doi.org/10.1002/2017JA024399

Santolík, O., & Gurnett, D. A. (2003). Transverse dimensions of chorus in the source region. *Geophysical Research Letters*, *30*, 1031. https://doi.org/10.1029/2002GL016178

Santolík, O., Gurnett, D. A., Pickett, J. S., Parrot, M., & Cornilleau-Wehrlin, N. (2003). Spatio-temporal structure of storm-time chorus. *Journal of Geophysical Research*, *108*, 1278. https://doi.org/10.1029/2002JA009791

Shen, X.-C., Li, W., Ma, Q., Agapitov, O., & Nishimura, Y. (2019). Statistical analysis of transverse size of lower band chorus waves using simultaneous multisatellite observations. *Geophysical Research Letters*, *46*(11), 5725–5734. https://doi.org/10.1029/2019GL083118

Shiokawa, K., Katoh, Y., Hamaguchi, Y., Yamamoto, Y., Adachi, T., Ozaki, M., et al. (2017). Ground-based instruments of the PWING project to investigate dynamics of the inner magnetosphere at subauroral latitudes as a part of the ERG-ground coordinated observation network. *Earth Planets and Space*, *69*(1), 160. https://doi.org/10.1186/s40623-017-0745-9

Summers, D., Ni, B., & Meredith, N. P. (2007). Timescales for radiation belt electron acceleration and loss due to resonant wave-particle interactions: 2. Evaluation for VLF chorus, ELF hiss, and electromagnetic ion cyclotron waves. *Journal of Geophysical Research*, *112*(A4), A04207. https://doi.org/10.1029/2006JA011993

Thorne, R., Li, W., Ni, B., Ma, Q., Bortnik, J., Chen, L., et al. (2013). Rapid local acceleration of relativistic radiation-belt electrons by magnetospheric chorus. *Nature*, *504*(7480), 411–414. https://doi.org/10.1038/nature12889

Titova, E. E., Kozelov, B. V., Jiriček, F., Smilauer, J., Demekhov, A. G., & Trakhtengerts, V. Y. (2003). Verification of the backward wave oscillator model of VLF chorus generation using data from MAGION 5 satellite. *Annales Geophysicae*, *21*, 1073–1081. https://doi.org/10.5194/angeo-21-1073-2003

Tsurutani, B. T., & Smith, E. J. (1974). Postmidnight chorus: A substorm phenomenon. *Journal of Geophysical Research*, *79*(1), 118–127. https://doi.org/10.1029/JA079i001p00118

Tsurutani, B. T., & Smith, E. J. (1977). Two types of magnetospheric ELF chorus and their substorm dependences. *Journal of Geophysical Research*, *82*(32), 5112–5128. https://doi.org/10.1029/JA082i032p05112

Tsyganenko, N. A. (2002). A model of the near magnetosphere with a dawn-dusk asymmetry: 1. Mathematical structure. *Journal of Geophysical Research*, *107*(A8), 1179. https://doi.org/10.1029/2001JA000219

Yagitani, S., Habagishi, T., & Omura, Y. (2014). Geotail observation of upper band and lower band chorus elements in the outer magnetosphere. *Journal of Geophysical Research: Space Physics*, *119*(6), 4694–4705. https://doi.org/10.1002/2013JA019678

Yamaguchi, K., Matsumuro, T., Omura, Y., & Nunn, D. (2013). Ray tracing of whistler-mode chorus elements: Implications for generation mechanisms of rising and falling tone emissions. *Annales Geophysicae*, *31*(4), 665–673. https://doi.org/10.5194/angeo-31-665-2013